IEEE Transactions on Power Electronics, pp. 1–1, 2020

Comprehensive Spectral Analysis of PWM Waveforms With Compensated DC link Oscillations

S. Milovanovic and D. Dujic

POWER ELECTRONICS LABORATORY
ÉCOLE POLYTECHNIQUE FÉDÉRALE DE LAUSANNE

This article has been accepted for publication in a future issue of this journal, but has not been fully edited. Content may change prior to final publication. Citation information: DOI 10.1109/TPEL.2020.2996418, IEEE Transactions on Power Electronics

Comprehensive Spectral Analysis of PWM Waveforms With Compensated DC link Oscillations

Stefan Milovanović, *Student Member, IEEE,* Dražen Dujić, *Senior Member, IEEE*
Power Electronics Laboratory, École Polytechnique Fédérale de Lausanne
stefan.milovanovic@epfl.ch; drazen.dujic@epfl.ch

***Abstract*—In the available literature, including reference books on the topic, the spectral analysis of voltage waveforms obtained through the use of pulse-width modulation relies on the assumption of an ideally flat voltage across the DC link of a considered switching structure. Nevertheless, certain converter families (e.g. modular multilevel converter, characterized by the presence of distributed and floating DC links), feature low frequency oscillations of DC voltage within their switching stages. On these terms, the flat DC link assumption cannot be considered valid from both theoretical and practical viewpoints. In case carrier-based modulation is employed, unless properly compensated through the modulation signal adjustments, the above mentioned voltage oscillations cause undesirable distortion of the converter currents. However, the very same adjustments of modulation signals introduce additional challenges in the spectral analysis of the voltage across the AC terminals of an observed switching stage. This paper provides the AC terminals voltage analysis of a single half-bridge experiencing DC link oscillations, which are compensated through the modulation signal generation process. Pulse-width modulation with the conventional triangular carrier is considered, while all the results are presented in a generalized form, making them easily extendable to cascaded structures. All of the presented results were experimentally validated.**

***Index Terms*—Pulse Width Modulation (PWM), Carrier-based modulation, DC link oscillations, Modular Multilevel Converter (MMC), Chainlink converters**

I. Introduction

Carrier-based modulation schemes represent the most popular means of synthesizing the desired voltage references of both monolithic and modular power converters. **Fig. 1** depicts a phase leg of the conventional Two-Level (2LVL) Voltage Source Converter (VSC), where power semiconductor switching signals are generated through the comparison of an arbitrary reference signal, henceforth referred to as the modulation signal $m(t)$, and the carrier signal $C(t)$ taking either the sawtooth or the triangular shape [1]. As can be seen from **Fig. 2**, whenever the value of the modulation signal exceeds the value of the carrier, the upper switch of the phase-leg presented in **Fig. 1** gets turned on and vice versa. Consequently, the leg switching function $p(t)$ represents a pulse train with the width of pulses varying depending on the value of the modulation signal. Hence the well known name Pulse-Width Modulation (PWM).

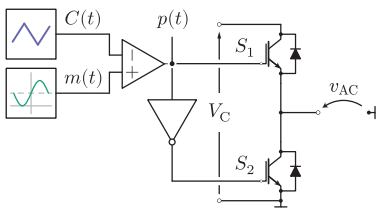

Fig. 1. Phase leg of a conventional 2LVL VSC

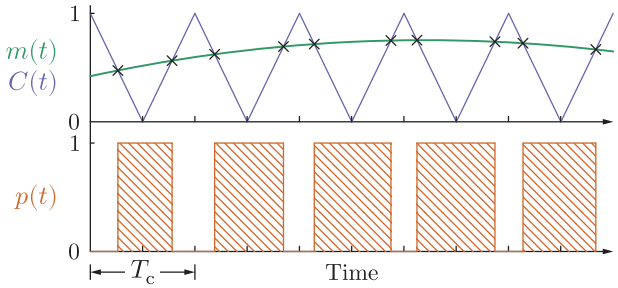

Fig. 2. Typical pulse train created through the comparison of a modulation signal and the triangular carrier

Until now, two main approaches towards the spectral analysis of a 2LVL VSC leg AC voltage v_{AC} have been adopted. The first one relies on the creation of the so-called unit cell from where two dimensional Fourier expansion can be applied [1]–[3]. The second approach utilizes a set of convenient mathematical observations, which allow identical results to be obtained, however, with the use of much simpler and more intuitive single dimensional Fourier series [4], [5]. It is noteworthy that both approaches assume a perfectly flat voltage V_{C} across the DC terminals of the converter leg presented in **Fig. 1**. Such an assumption can be considered reasonable under a certain set of scenarios. For instance, it is well known that in the conventional Three-Phase (3PH) 2LVL VSC, the capacitor mounted in the DC link conducts only high frequency current (which corresponds to the converter DC current ripple originating from the joint switching of multiple phase legs). Therefore, even with a modest DC link capacitance, the DC link voltage oscillations can be mitigated to a negligible level.

On the other hand, the chainlink converters employing distributed DC links, such as the Modular Multilevel Converter (MMC) [6], [7] or the Cascaded H-Bridge (CHB) converter [8], experience the inevitable DC link oscillations, irrespective of the capacitance installed in the converter building blocks, as the load current segments flow directly through it. **Fig. 3** presents an MMC phase leg realized by stacking the so-called submodules (SMs) [9], which are normally found in either Half-Bridge (HB) or Full-Bridge (FB) configuration, in series.

This article has been accepted for publication in a future issue of this journal, but has not been fully edited. Content may change prior to final publication. Citation information: DOI 10.1109/TPEL.2020.2996418, IEEE Transactions on Power Electronics

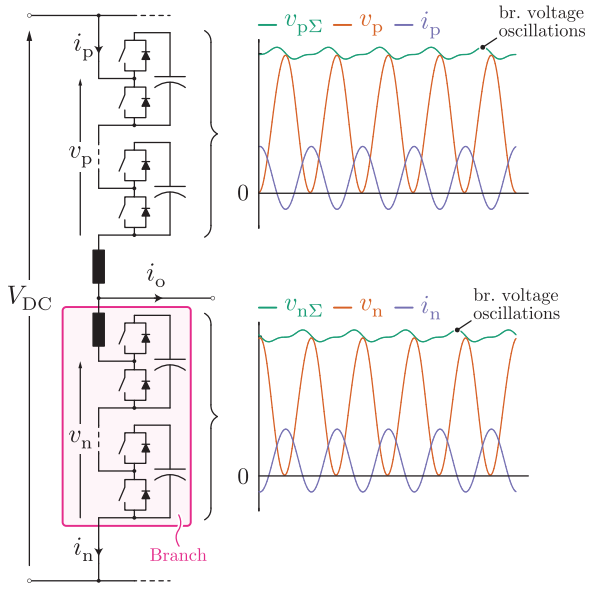

Fig. 3. Phase leg of an MMC employing HB SMs. Please notice that SMs represent floating energy sources. Therefore, oscillations across their DC links can be mitigated to a reasonable level by a proper choice of the capacitance [11], [12]. Nevertheless, these oscillations cannot be avoided.

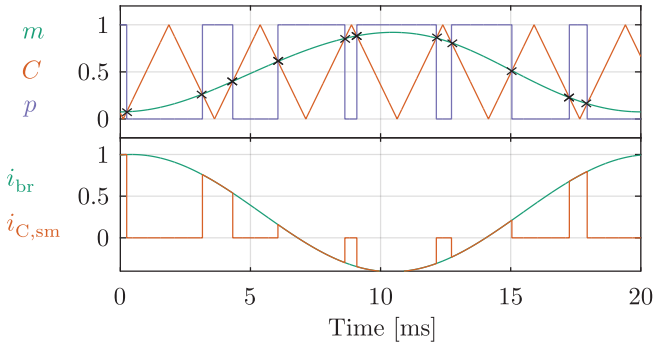

Fig. 4. Typical shape of an SM capacitor current ($i_{C,sm}$) in case carrier-based modulation is used to synthesize the SM voltage references. All the currents were normalized with respect to the branch maximum current.

SMs represent floating energy sources with capacior currents corresponding to the chopped branch current, as depicted in **Fig. 4**. Consequently, the SM capacitor voltage oscillates at frequencies corresponding to the multiples of the leg output current denoted by i_o [10]. Henceforward, these oscillations will be classified as low frequency oscillations. However, constraining these oscillations to a negligible level results in substantially high capacitance demands, which in turn results in high converter cost. Thus, oscillations in the range of $\pm 10\%$ (or less) of the nominal SM voltage are normally tolerated.

Unless compensated through an adequate modulation/control scheme, these low frequency oscillations cause the distortion of the converter currents. For instance, undesired oscillations of the MMC branch currents, at twice the converter output current frequency, are a well known phenomenon in case the so-called direct modulation, where no adjustments of the modulation signals are taken into account, is used [13]–[15]. In [16], [17] suppression of the undesired branch current oscillations, ensured through the use of additional controllers, was thoroughly discussed. An alternative to the approach relying on the use of additional controllers implies the modulation signals adjustment based on the available measurements of the SM DC link voltages, as presented in [10]. As a result, the branch current distortions are avoided [15]. Notwithstanding, such a compensation requires the modulation signal to deviate from the signal requested by the controller (normally sinusoidal), which introduces additional challenges in the spectral analysis of the SM terminals voltage.

Acquiring the knowledge on the spectral content of the converter switching stages, irrespective of the converter nature, is considered to be of importance for a few reasons. Generation of modulation signals, with the aim of synthesizing desired references at the frequency of the converter currents, does not consider the higher order harmonics generated in the switching stage voltages. It is exactly the set of higher order harmonics that affects the converter current ripples, meaning that proper sizing of the converter must take these ones into account. Further, the chainlink converters, such as the MMC, provide various degrees of freedom with respect to shaping of the voltage seen from the converter terminals. For instance, a thorough analysis of the MMC operating with phase-shifted carriers and direct modulation can be found in [18]. However, the corrections in the SM modulation signals, generated to suppress the converter current distortions, were not analyzed. Neglecting the oscillations of the SM DC links, as well as the means for addressing it, results in the wrong conclusions regarding the spectral content observed in the chainlink converters operating in the closed-loop. Even though the MMC was used as an exemplary case during the previous discussions, identical reasoning can be applied to the other converters with the similar nature (i.e. ⅄ or Δ STATCOM [19], CHB converter, Hexverter [20], Matrix MMC [21], etc.).

To provide the framework for the analysis of any chainlink structure, a detailed analysis of its basic building blocks must be conducted beforehand. This paper presents a thorough mathematical analysis of voltage generated across the AC terminals of the very basic switching structure - the HB SM. The expressions derived throughout the following sections can be used to expand the analysis onto a more complicated structure, such as the FB SM, an MMC branch, or even a whole MMC leg. The DC link oscillations occurring at multiples of the converter AC current frequency, being compensated by an appropriate modulation signal adjustments, are taken into account. Even though this paper leans on the analysis presented in [4], [5], it provides a comprehensive extension to the cases where the switching stage DC voltage is not ideally flat. Thus, its main contributions can be summarized as:

- DC link oscillations in the HB switching leg are taken into account in the spectral analysis of its AC voltage. In contrast to the analyses being available in the literature, corrections of the modulation signals, based on the SM DC link voltage measurements, are treated for the first time and their influence on the converter voltage spectra is outlined.
- Derivation of results is performed in a generalized manner. Therefore, vast variety of structures can be analyzed in a similar fashion.

This article has been accepted for publication in a future issue of this journal, but has not been fully edited. Content may change prior to final publication. Citation information: DOI 10.1109/TPEL.2020.2996418, IEEE Transactions on Power Electronics

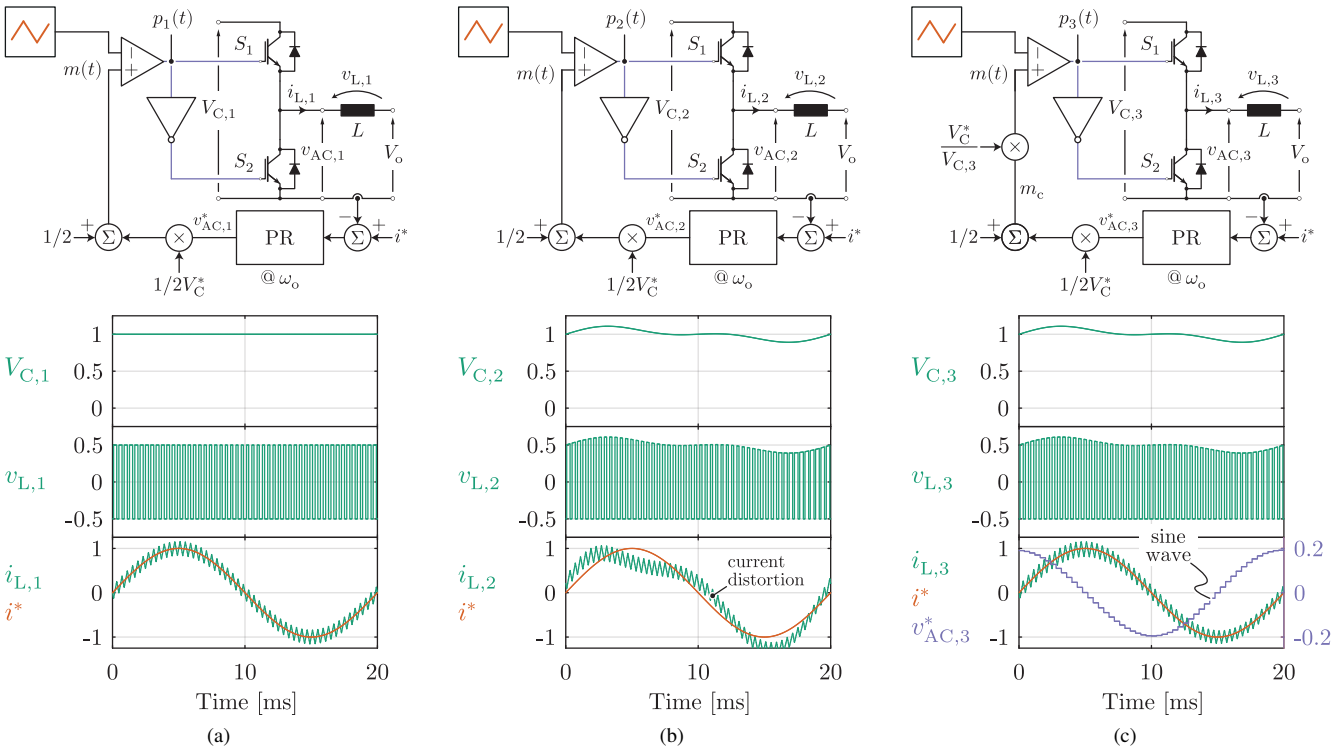

Fig. 5. An exemplary circuit used to illustrate the importance of compensating the HB DC link oscillations through the modulation signal adjustments. Voltages and currents are defined in per unit metrics, whereas the inductance was set such that its impedance equals 10% of the base impedance. In order to control the inductor current, the PR controller, tuned to the fundamental frequency ω_o is used in all the cases. (a) As can be seen, flat DC link voltage does not cause any distortions in the converter output current owing to the structure of the employed controller; (b) Since the PR controller is not tuned to suppress the effects of the DC link voltage disturbances, the inductor current becomes distorted. As discussed throughout this section, such an issue can be overcome either by employing a set of additional resonant parts in the PR controller or through the modulation signal adjustments; (c) Outcome of the modulation signal adjustments based on the DC link voltage measurements. Even though the PR controller is tuned only to the fundamental frequency, oscillations in the DC link are compensated through the modifications of modulation signal corresponding to the output of the controller m_c. As a result, the current of the observed HB is not distorted.

II. DC LINK OSCILLATIONS COMPENSATION THROUGH THE MODULATION SIGNAL ADJUSTMENTS

The aim of this section is to present the need for the adjustments of the converter modulation signal in case its DC link experiences low frequency oscillations. For that matter, one can observe an exemplary circuit depicted in **Fig. 5**. It consists of a single HB SM, a filter inductor L and a constant DC voltage source $V_o = 0.5$ p.u. To control the filter inductor current, the PR controller tuned to the fundamental frequency, denoted by ω_o, is utilized. According to **Fig. 2**, the HB switching signals (p for the switch S_1 and its complementary $\overline{p}$ for the switch S_2) are generated by comparing the modulation signal m with the triangular carrier. Consequently, the voltage across the AC terminals of the observed HB equals

$$v_{AC} = p \times V_C \tag{1}$$

According to [1]–[5], the bridge switching function p can be expanded as (2), where the term denoted by H represents all of the higher order harmonics present in p.

$$p = \underbrace{m}_{\substack{\text{modulation}\\ \text{signal}}} + \underbrace{H}_{\substack{\text{higher order}\\ \text{harmonics}}} \tag{2}$$

Substitution of (2) into (1) enables the qualitative analysis of voltage generated across the AC terminals of the HB presented in **Fig. 5**. In case an ideally flat voltage $V_{C,1} = V^*_C = 1$ p.u is applied across the DC terminals of the observed HB, as depicted in **Fig. 5a**, the PR controller outputs a sinusoidal signal. Thus, the modulation signal is set as $m_1 = \frac{1}{2} + \frac{\hat{m}}{2}\cos(\omega_o t)$, meaning that the voltage across the filter inductor equals

$$v_{L,1} = \frac{\hat{m}}{2}\cos(\omega_o t) + H_1 \tag{3}$$

Consequently, the converter output current contains the fundamental frequency component, along with the ripple depending on the filter inductance and the voltage component denoted by H_1, as presented in **Fig. 5a**.

In case the DC link of the observed HB comprises low frequency oscillations, which can be formulated as $V_{C,2} = 1 + \sum_{n=1}^{\infty} \hat{V}^{(n)}_{C,2}\cos(n\omega_o t + \Psi_n)$, while retaining the PR controller used in **Fig. 5a**, the filter inductor current becomes distorted. **Fig. 5b** demonstrates such a case, where, for illustration purposes, the converter DC link voltage was set as $V_{C,2} = 1 + \frac{1}{2}\{0.15\cos(\omega_o t) + 0.1\cos(2\omega_o t)\}$. Apparently, low frequency oscillations in the DC link have negative impact on the inductor current control. To suppress the undesired current oscillations, originating from the low frequency oscillations in the DC link, the PR controller depicted in

Fig. 5b must be extended by additional resonant parts, as presented in **Fig. 6**. Spectral analysis of PWM waveforms generated according to such an approach was presented in [22]. Nevertheless, the same goal can be achieved in case the modulation signal corrections, presented in **Fig. 5c**, are performed. It is noteworthy that the low frequency oscillations in the DC link of any switching stage occur whenever it processes the energy as an independent Single-Phase (1PH) converter. The MMC represents a well known exemplary case, whereas the above statement can be confirmed by observing the waveforms provided in **Figs. 3** and **4**.

As can be seen from the bottom-most plot of **Fig. 5c**, the current controller outputs a sinusoidal signal comprising only the fundamental frequency, leading to simpler and more elegant solution compared to the current controller extension. Prior to entering the modulator, the signal corresponding to the controller output m_c gets multiplied with the voltage of the perfectly flat DC link V_c^* and divided by the actual DC link voltage measurement $V_{\mathrm{C},3}$, leading to (4). In other words, the signal entering the modulator differs from the modulation signal demanded by the system controllers.

$$m_3 = \left\{ \frac{1}{2} + \underbrace{\frac{\hat{m}}{2}\cos(\omega_\mathrm{o} t)}_{\substack{\text{from the ind.}\\ \text{current ctrl.}}} \right\} \underbrace{\frac{V_\mathrm{C}^*}{V_{\mathrm{C},3}}}_{\text{adjust.}} \tag{4}$$

The closed-loop control of the MMC [10] implies the modulation signals generation in the identical fashion. Therefore, although simplified, the example presented in **Fig. 5** covers a significant span of realistic cases. Further, the substitution of (2) and (4) into (1) yields

$$v_{\mathrm{L},3} = \frac{\hat{m}}{2}\cos(\omega_\mathrm{o} t) + H_3 V_{\mathrm{C},3}, \tag{5}$$

from where it can be seen that the low frequency oscillations in the AC current of the analyzed bridge are indeed eliminated. Yet, on these terms, the function describing the HB AC voltage differs from the case assuming the flat DC link voltage. Consequently, a new approach towards such an analysis is required and it is exactly the topic being addressed in the following sections. As $v_{\mathrm{AC},3} = p_3 \times V_{\mathrm{C},3}$, a detailed investigation of this voltage component requires the switching function p_3 to be completely known.

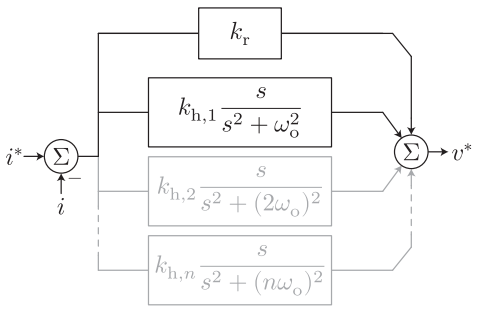

Fig. 6. Unless the low frequency oscillations in the DC link are compensated through the modulation signal corrections, the PR controller used in **Fig. 5b** must be extended by additional resonant parts. However, the frequency of undesired current oscillations must be known in advance should the presented controller be successfully used.

III. Derivation of relevant spectral components

A. Natural sampling

In case the HB switching stage is considered, it can be shown, according to [5], that an expansion of a PWM waveform p, obtained by comparing an arbitrary modulation signal m^* with a triangular carrier, can be performed as

$$p = m^* - \frac{j}{2\pi}\sum_{\substack{k=-\infty\\ k\neq 0}}^{\infty} \frac{(-1)^k}{k} e^{jk\omega_\mathrm{c} t} e^{-jk\gamma_\mathrm{c}} \left\{ e^{jk\pi m^*} - e^{-jk\pi m^*} \right\}, \tag{6}$$

where ω_c and γ_c denote the frequency and the phase-shift of the observed carrier.

At first instance, let one observe the term $e^{jk\pi m^*}$. Namely, in case $m^* = \frac{1}{2} + \frac{\hat{m}}{2}\cos(\omega_\mathrm{o} t)$, this term can be effortlessly expanded by means of the Jacobi-Anger expansion (7), where J_n denotes the Bessel function of the first kind.

$$e^{jk\cos(\theta)} = \sum_{n=-\infty}^{\infty} j^n J_n(k) e^{jn\theta} \tag{7}$$

However, generation of the modulation signal according to (4) prevents the use of (7). By rewriting (4) as

$$m = \frac{\frac{1}{2} + \frac{\hat{m}}{2}\cos(\omega_\mathrm{o} t)}{1 + \sum_{n=1}^{\infty} \hat{v}_{\mathrm{C},n}\cos(n\omega_\mathrm{o} t + \Psi_n)}, \tag{8}$$

one can conclude that an expansion similar to (7) requires the integral defined in (9) to be solved. Unfortunately, such an integral does not have a simple explicit solution. Therefore, another method of expanding (6) needs to be employed.

$$A_k = \frac{1}{T_\mathrm{o}} \int_{-\frac{T_\mathrm{o}}{2}}^{\frac{T_\mathrm{o}}{2}} e^{j\left(\frac{\hat{m}\cos(\omega_\mathrm{o} t)}{2(1+\sum_{n=1}^{\infty} \hat{v}_{\mathrm{C},n}\cos(n\omega_\mathrm{o} t + \Psi_n))} - k\omega_\mathrm{o} t \right)} \mathrm{d}t \tag{9}$$

The modulation signal defined in (8) represents a function with period equal to $T_\mathrm{o} = 2\pi/\omega_\mathrm{o}$. Hence, it can also be expanded as $m^* = m_0 + \sum_{i=1}^{\infty} \hat{m}_i \cos(i\omega_\mathrm{o} t + \zeta_i)$. On these terms, the modulation signal becomes composed of an infinite sum of periodic signals. Hence, the expansion defined in (7) cannot be used. However, a convenient mathematical transformation, presented in (10), can be performed.

$$\begin{aligned} e^{jk\pi m^*} &= e^{jk\pi m_0} e^{jk\pi \sum_{i=1}^{\infty} \hat{m}_i \cos(i\omega_\mathrm{o} t + \zeta_i)} \\ &= e^{jk\pi m_0} \prod_{i=1}^{\infty} e^{jk\pi \hat{m}_i \cos(i\omega_\mathrm{o} t + \zeta_i)} \end{aligned} \tag{10}$$

An important observation can be made from the above equation. Firstly, the function $e^{jk\pi m^*}$, which is the crucial term of (6), can be represented by the product of terms being expandable in the form of (7). Secondly, the analysis of the switching function p can also be performed in the frequency domain, where an infinite product can be replaced with an infinite array of convolutions [4], [5]. Translating (6) into the frequency domain, while recalling that $\mathcal{F}\{e^{jk\omega_\mathrm{c} t} f(t)\} = F(\omega - k\omega_c)$, provides one with

This article has been accepted for publication in a future issue of this journal, but has not been fully edited. Content may change prior to final publication. Citation information: DOI 10.1109/TPEL.2020.2996418, IEEE Transactions on Power Electronics

$$P(\omega) = M^*(\omega) - \frac{j}{2\pi}\sum_{\substack{k=-\infty \\ k\neq 0}}^{\infty}\frac{(-1)^k}{k}e^{-jk\gamma_c}\times$$
$$\left[\mathcal{F}\left\{e^{jk\pi m^*}\right\}(\omega-\omega_c) - \mathcal{F}\left\{e^{-jk\pi m^*}\right\}(\omega-\omega_c)\right] \quad (11)$$

Proceeding with the intended analyses requires a further investigation of the function $\mathcal{F}\left\{e^{jk\pi m^*}\right\}$. According to the convolution theorem, $\mathcal{F}\{x(t)\times y(t)\} = \frac{1}{2\pi}X(\omega) * Y(\omega)$, where $x(t) \leftrightarrow X(\omega)$ and $y(t) \leftrightarrow Y(\omega)$. Consequently, (12) can be derived for the case considering the representation of the modulation signal with a finite number of components denoted by N.

$$\mathcal{F}\left\{e^{jk\pi m^*}\right\} = \frac{e^{jk\pi m_0}}{(2\pi)^{N-1}}\left[\mathcal{F}\left\{e^{jk\pi\hat{m}_1\cos(\omega_o t+\zeta_1)}\right\} * \cdots *\right.$$
$$\left.\mathcal{F}\left\{e^{jk\pi\hat{m}_N\cos(N\omega_o t+\zeta_N)}\right\}\right] \quad (12)$$

Also, combining (7) with the fact that $e^{j\omega_k t} \leftrightarrow 2\pi\delta(\omega-\omega_k)$, leads to (13).

$$\mathcal{F}\left\{e^{jk\pi\hat{m}_i\cos(i\omega_o t+\zeta_i)}\right\} = \sum_{n=-\infty}^{\infty} j^n J_n(k\pi\hat{m}_i)e^{jn\zeta_i}2\pi\delta(\omega-ni\omega_o) \quad (13)$$

At this point, all the conditions for a general expansion of (12) are fulfilled. For this purpose, the mathematical induction method can be employed. Consequently, there is the need to look for the convolution of two and three functions, having the form of (13), as presented in (14) and (15), respectively. From there, one can easily derive an expression describing the convolution of an infinite number of functions having the form of (13). Nevertheless, such an approach would be rather impractical given that it requires an infinite number of sums to be incorporated into the calculations. On the other hand, achieving a satisfactory precision in the representation of the modulation signal can quite often be guaranteed with the use of only N terms in the product given in (10).

To determine a sufficient number of terms representing the modulation signal from (8), an exemplary case provided in **Fig. 7** can be analyzed. For the sake of comparison, a modulation signal generated by neglecting the oscillations of the DC link voltage will be denoted by m_o^*, whereas its counterpart obtained as (4) will be denoted by m_Σ^*. As can be seen, there is a clear difference between these two signals in both time and frequency domain. However, **Fig. 7b** shows that the signal m_Σ^* can be represented with a limited number of harmonics. Therefore, expression (12) can be used, whereas

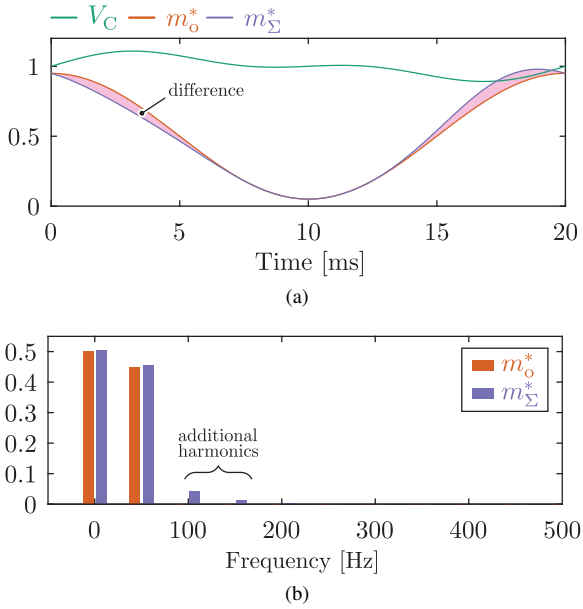

Fig. 7. For the sake of modulation signals comparison, the DC link voltage was set as $V_C = 1 + \frac{1}{2}\{0.15\cos(\omega_o t) + 0.1\cos(2\omega_o t)\}$, whereas the modulation signal corresponding to the controller output was adopted as $m_o^* = 0.5(1 + 0.9\cos(\omega_o t)$. As can be seen, compensating the DC link voltage oscillations in m_Σ^* introduces additional harmonics into the analysis. Moreover, the frequency domain image of m_Σ^* indicates that this signal comprises a limited number of dominant harmonics (despite consisting of an infinite number of terms). Therefore, (12) can be utilized with the satisfactory precision.

the satisfactory precision can be achieved by expressing the modulation signal as

$$m_\Sigma^* \approx m_0 + \sum_{i=1}^{3}\hat{m}_i\cos(i\omega_o t + \zeta_i), \quad (17)$$

where all the coefficients (m_i and ζ_i) can be easily obtained for any of the converter operating points. Replacing the coefficients from (17) into (15) and after a set of tedious mathematical manipulations, the converter switching function can be obtained as (18). When comparing (18) to the expressions already known in the literature [1], [5], it can be seen that additional harmonic components in the switching stage AC voltage are generated. In case the DC link voltage is flat, (18) can easily be rearranged to match the already known expressions. Namely, the modulation signal parameters can be set as $\{m_0, \hat{m}_1, \hat{m}_2, \hat{m}_3\} = \{1/2, \hat{m}, 0, 0\}$, while $\zeta_i = 0$, from where (19) can be obtained.

$$\mathcal{F}\left\{e^{jk\pi\hat{m}_i\cos(i\omega_o t+\zeta_i)}\right\} * \mathcal{F}\left\{e^{jk\pi\hat{m}_p\cos(p\omega_o t+\zeta_p)}\right\} = \sum_{n=-\infty}^{\infty}\sum_{q=-\infty}^{\infty}(2\pi)^2 j^{(n+q)}J_n(k\pi\hat{m}_i)J_q(k\pi\hat{m}_p)e^{j(n\zeta_i+q\zeta_p)}\delta(\omega-(ni+qp)\omega_o) \quad (14)$$

$$\mathcal{F}\left\{e^{jk\pi\hat{m}_i\cos(i\omega_o t+\zeta_i)}\right\} * \mathcal{F}\left\{e^{jk\pi\hat{m}_p\cos(p\omega_o t+\zeta_p)}\right\} * \mathcal{F}\left\{e^{jk\pi\hat{m}_r\cos(r\omega_o t+\zeta_r)}\right\} =$$
$$= \sum_{z=-\infty}^{\infty}\sum_{n=-\infty}^{\infty}\sum_{q=-\infty}^{\infty}(2\pi)^3 j^{(z+n+q)}J_z(k\pi\hat{m}_r)J_n(k\pi\hat{m}_i)J_q(k\pi\hat{m}_p)e^{j(n\zeta_i+q\zeta_p+z\zeta_r)}\delta(\omega-(zr+ni+qp)\omega_o) \quad (15)$$

$$p = m^* + \frac{2}{\pi}\sum_{k=1}^{\infty}\sum_{z=-\infty}^{\infty}\sum_{q=-\infty}^{\infty}\sum_{n=-\infty}^{\infty}\frac{(-1)^k}{k}J_z(k\pi\hat{m}_3)J_q(k\pi\hat{m}_2)J_n(k\pi\hat{m}_1)\sin\left(k\pi m_0+\frac{z+q+n}{2}\pi\right)\times$$
$$\cos([k\omega_c+(3z+2q+n)\omega_\mathrm{o}]t-k\gamma_\mathrm{c}+(z\zeta_3+q\zeta_2+n\zeta_1)) \quad (18)$$

$$p = m^* + \frac{2}{\pi}\sum_{k=1}^{\infty}\sum_{n=-\infty}^{\infty}\frac{(-1)^k}{k}J_n(k\pi\hat{m})\sin\left(\frac{k+n}{2}\pi\right)\cos([k\omega_c+n\omega_\mathrm{o}]t-k\gamma_\mathrm{c}) \quad (19)$$

Finally, once the HB switching function is known, its AC voltage can be calculated according to (1). Moreover, for any converter type, the procedure demonstrated above can be repeated in the steps summarized as:

1) Define the converter parameters (S_nom, L, v_grid, etc.).
2) Define a desired operating point.
3) For a given operating point, calculate the modulation signal m_o^*, currents, voltages and the DC link oscillations.
4) Calculate modulation signal m_Σ which takes the DC link oscillations into account.
5) Expand the calculated modulation signal into Fourier series. Determine the sufficient number of harmonics ensuring its satisfactory representation.
6) By following the logic presented in (14) and (15), derive (12) for the particular case.
7) Rearrange the frequency domain expression to obtain the expression resembling (18). Keep in mind that the number of sums in such an expression depends on the number of harmonic components used to represent the modulation signal. In general, the number of sums (n_sum) in the equation describing the HB switching function p equals to the number of harmonic components used to represent the modulation signal (N) plus one ($n_\mathrm{sum} = N + 1$).

An important remark regarding the calculation of the DC link voltage oscillations must be made. As stated in **Sec. II**, whenever an analyzed switching stage processes 1PH power, which is typical for the chainlink converters, the DC link oscillations at multiples of the fundamental frequency are observed. Further, as illustrated in **Fig. 4** on the example of an MMC SM, the DC link current of the analyzed structure contains switching harmonics. Nonetheless, one should always keep in mind that sizing of the DC link capacitance, in the applications falling within the scope of this paper, must ensure the desired limitation of the low frequency voltage components. Therefore, the DC link capacitance acts as a low-pass filter for the switching harmonics in the DC link current. To put it differently, the switching harmonics in the DC link voltage are normally negligible with respect to the low frequency oscillations caused by the 1PH power transfer at the AC terminals of the analyzed switching structure.

To provide the validation of the previous statements, **Fig. 8** presents the DC voltage of the SMs in the 0.5MW MMC, connected to the 5.6kV DC grid and operating with the carrier frequency equal to $f_\mathrm{c} = 385$Hz. As can be seen, even with the low switching frequency, the switching harmonics in the observed SMs fall significantly bellow the low frequency oscillations being in the focus of this paper. To summarize, the DC link voltage, used for the modulation signal correction, can be obtained from the averaged model of an arbitrary switching stage, without compromising the correctness of the derived results. Furthermore, in the chainlink converters, all the switching blocks, irrespective of their nature, belonging to the same string, receive the identical modulation signal. Therefore, all the blocks experience the same low frequency voltage oscillations, which can be calculated from the converter averaged models. As a result, the voltage spectrum of the whole string can be calculated by summing (18) written for every individual block. Consequently, highly modular topologies can be investigated, once the methodology suitable for the analysis of the basic building block spectrum is adopted.

B. Regular sampling

Generation of voltage across the terminals of a digitally controlled converter implies sampling of its modulation signal. Symmetric regular sampling implies sampling of the modulation signal every time the carrier signal reaches one or zero, depending on the choice. Once sampled, this value of the modulation signal is held constant for the rest of the converter switching period T_c, as presented in **Fig. 9**. Similarly, the asymmetric regular sampling allows for the sampling of modulation signal twice per switching period.

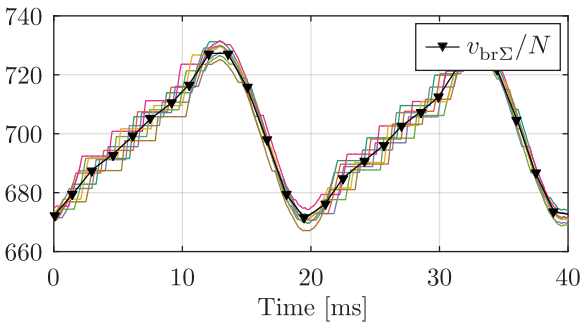

Fig. 8. SM capacitor voltages in the 0.5MW 3PH MMC operating with the carrier frequency equal to $f_\mathrm{c} = 385$Hz and $N_\mathrm{SM} = 8$ SMs per branch. The value of the SM capacitance was set as $C_\mathrm{SM} = 2.25$mF.

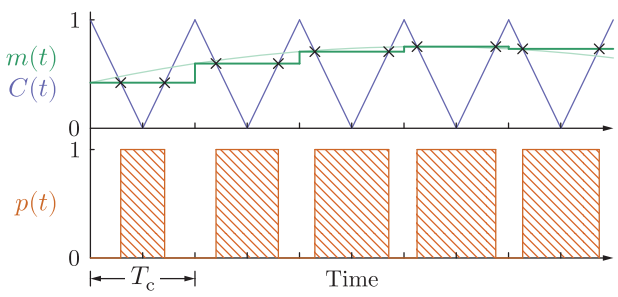

Fig. 9. PWM pulse train obtained through the comparison of a regularly sampled modulation signal and the triangular carrier

In other words, whenever the carrier reaches either zero or one, the modulation signal is sampled and held constant until the next sampling instant. In the following paragraphs, only the case of symmetric regular sampling is covered since the results can easily be adjusted to the case of asymmetric regular sampling. According to **Fig. 10**, sampling of an arbitrary signal $m(t)$ can be described as multiplication with an infinite set of Dirac functions, repeating with the sampling frequency $f_c = 1/T_c$, followed by the Zero Order Hold (ZOH) filter. It is straightforward to show that the frequency domain image of the sampled reference $m_s(t)$ can be expressed as (20).

$$M_s(\omega) = \frac{\sin(\frac{\omega T_c}{2})}{\frac{\omega T_c}{2}} e^{-j\omega\frac{T_c}{2}} \sum_{k=-\infty}^{\infty} M(\omega - k\omega_c) \tag{20}$$

Let the modulation signal be defined as (21). For an arbitrary frequency component $m_i(t)$ and a fixed value of $k \neq 0$, expression (20) can be rewritten as (22).

$$m(t) = m_0 + \sum_{i=1}^{N} \underbrace{\hat{m}_i \cos(i\omega_o t + \zeta_i)}_{m_i(t)} \tag{21}$$

$$M_{s,i}^{(k)}(\omega) = \pi\hat{m}_i \frac{\sin(\frac{\omega T_c}{2})}{\frac{\omega T_c}{2}} e^{-j\omega\frac{T_c}{2}} \Big\{ e^{j\zeta_i}\delta(\omega - k\omega_c - i\omega_o) + e^{-j\zeta_i}\delta(\omega - k\omega_c + i\omega_o) \Big\} \tag{22}$$

Since $k \in (-\infty, \infty)$, the term $M_{s,i}^{(-k)}(\omega)$ can be effortlessly obtained, which provides the means for straightforward calculation of $\mathcal{F}^{-1}\{M_{s,i}^{(k)}(\omega) + M_{s,i}^{(-k)}(\omega)\}$ as

$$\begin{aligned}\mathcal{F}^{-1}\{M_{s,i}^{(k)}(\omega) + M_{s,i}^{(-k)}(\omega)\} = \\ \hat{m}_i \frac{\sin([k\omega_c + i\omega_o]\frac{T_c}{2})}{[k\omega_c + i\omega_o]\frac{T_c}{2}} \cos([k\omega_c + i\omega_o](t - \frac{T_c}{2}) + \zeta_i) + \\ \hat{m}_i \frac{\sin([k\omega_c - i\omega_o]\frac{T_c}{2})}{[k\omega_c - i\omega_o]\frac{T_c}{2}} \cos([k\omega_c - i\omega_o](t - \frac{T_c}{2}) - \zeta_i)\end{aligned} \tag{23}$$

By combining (20) and (23), with subsequent translation into the time domain, one can obtain (24).

$$\begin{aligned} m_s(t) = m_0 + \sum_{i=1}^{N} \frac{\sin(\frac{i\omega_o T_c}{2})}{\frac{i\omega_o T_c}{2}} \hat{m}_i \cos(i\omega_o t + \zeta_i - \frac{i\omega_o T_c}{2}) + \\ \sum_{i=1}^{N}\sum_{k=1}^{\infty} \hat{m}_i \frac{\sin([k\omega_c + i\omega_o]\frac{T_c}{2})}{[k\omega_c + i\omega_o]\frac{T_c}{2}} \cos([k\omega_c + i\omega_o](t - \frac{T_c}{2}) + \zeta_i) + \\ \sum_{i=1}^{N}\sum_{k=1}^{\infty} \hat{m}_i \frac{\sin([k\omega_c - i\omega_o]\frac{T_c}{2})}{[k\omega_c - i\omega_o]\frac{T_c}{2}} \cos([k\omega_c - i\omega_o](t - \frac{T_c}{2}) - \zeta_i) \end{aligned} \tag{24}$$

As can be seen from the above equation, sampling of the modulation signal $m(t)$ creates additional harmonics in the signal entering the modulator. Also, (24) confirms the well known fact of the sampling block delaying the reference signal by half of the switching period [1]. As the modulation signal (24) can be represented by the sum of harmonic components, the methodology presented in **Sec. III-A** can be reused. In other words, regular sampling can be treated in the very same way as natural sampling, however, with additional harmonic components in the modulation signal. Similarly to the approach adopted in **Sec. III-A**, the number of harmonic components taken into account in (24) needs to be limited, otherwise (14) and (15) comprise infinite sums, which makes their use impractical. Additionally, the case of asymmetric regular sampling can be covered with the expression similar to (24), however, with the term $T_c/2$ being changed with $T_c/4$.

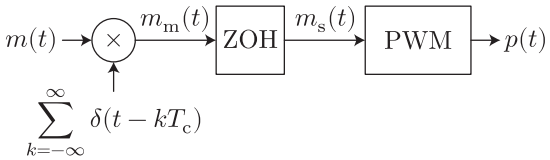

Fig. 10. Block diagram of the sampling process followed by the modulator

IV. Experimental Results

To verify the correctness of the results presented above, the laboratory setup, presented in **Fig. 11a**, was used. The HB module employed for this purpose was Imperix PEB 8032 [23], whereas Imperix B-Box [24] was used as a system controller. To obtain the experimental results, an open circuit (i.e no load at the HB AC terminals) was used. Loading the HB module with current, however, would have a certain effect on its output voltage spectrum, due to the effects related to the dead time [25]. Notwithstanding, these effects can be considered minor and not in the scope of this paper.

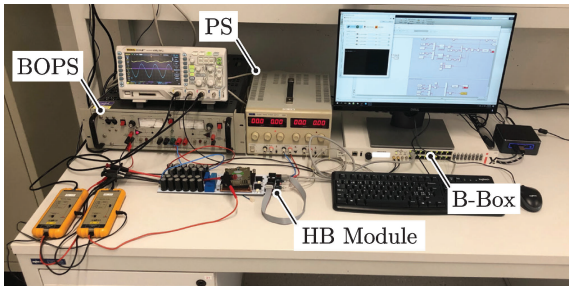

(a)

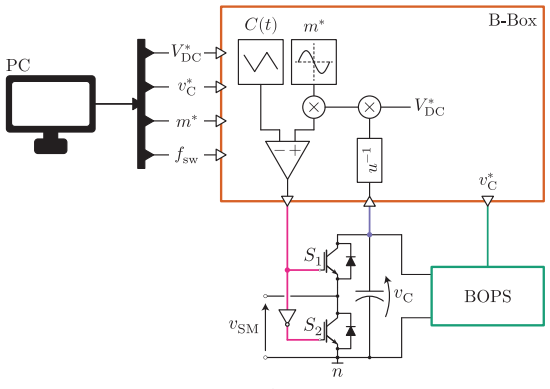

(b)

Fig. 11. (a) Laboratory setup; (b) Testing circuit diagram; Even though the B-Box generates the Bipolar Operational Power Supply (BOPS) output voltage reference, the DC link voltage used for the modulation signal corrections is obtained from the voltage sensor (LEM LV25-P) being a part of the employed HB module.

This article has been accepted for publication in a future issue of this journal, but has not been fully edited. Content may change prior to final publication. Citation information: DOI 10.1109/TPEL.2020.2996418, IEEE Transactions on Power Electronics

TABLE I: Properties of the used laboratory setup

Parameter	Label	Value
DC link nominal voltage	V^*_{DC}	45V
Fundamental frequency	f_{o}	50Hz
Switching frequency	f_{sw}	5kHz
Oscillations at $1 \times f_{\mathrm{o}}$	$\Delta\hat{v}_{\mathrm{AC},1}$	3.5V
Oscillations at $2 \times f_{\mathrm{o}}$	$\Delta\hat{v}_{\mathrm{AC},2}$	1.75V
Modulation signal	$\hat{m}$	0.9

The HB module DC link was connected to BOPS providing a voltage amplification of $G = 10$. Consequently, the HB DC link voltage can be controlled to follow an arbitrary reference. The BOPS voltage reference (25) was provided from the B-Box analog output, whereas the module logical circuitry was supplied by the test bench Power Supply (PS), as presented in **Fig. 11a**. **Fig. 11b** contains the testing circuit diagram, while all the parameters relevant for the conducted experiment can be found in **Tab. I**. Despite the BOPS voltage reference being supplied by the B-Box, the DC link voltage measurements are acquired exclusively through the voltage sensor (LEM LV25-P) hosted by the employed HB module. In other words, the modulation signal adjustments were truly performed in the closed-loop manner.

$$V_{\mathrm{C}} = V^*_{\mathrm{DC}} + \Delta\hat{v}_{\mathrm{AC},1}\cos(\omega_{\mathrm{o}}t) + \Delta\hat{v}_{\mathrm{AC},2}\sin(2\omega_{\mathrm{o}}t) \quad (25)$$

As stated in **Sec. III-A**, expressions derived throughout this paper can be easily adjusted for the use in the cases already covered in the literature. Therefore, **Fig. 12** presents the results obtained in case no voltage oscillations are present in the DC link of the HB module. In other words, $\Delta\hat{v}_{\mathrm{AC},1} = 0$ and $\Delta\hat{v}_{\mathrm{AC},2} = 0$. **Fig. 12a** presents the module DC link voltage along with the modulation signal set as $m = 0.5 + 0.45 \times \cos(2\pi 50t)$. **Fig. 12b** provides the comparison of the results obtained by means of the derived analytic expressions (18) and (24), which are modified in accordance with **Sec. III-A**, and the voltage measured across the module's AC terminals. A slight mismatch between the analytic and experimental results can be observed. However, such a mismatch can be attributed to the effects not being taken into account by the conducted analyses (for instance, voltage drop across the switches of the used HB module, deadtime, non-perfect voltage/current measurement, etc.).

In the next step, voltage oscillations in the DC link of the used HB module were intentionally generated, as presented in **Fig. 13a**. Additionally, the modulation signal retained the shape already presented in **Fig. 12a**. Consequently, a set of harmonics at two and three times the fundamental frequency becomes observable in the voltage measured/calculated across the module's AC terminals, as demonstrated in **Fig. 13b**.

To avoid the low frequency components in the HB module AC voltage, its DC link voltage was measured and fed back to the B-Box in order to adjust the modulation signal in accordance with (4). **Fig. 14a** presents the shape of the modified modulation signal, while the modulation signal from **Fig. 13a** was intentionally included in the same plot and colored in gray for the sake of comparison. **Fig. 14b** presents the comparison between the analytic and experimental results. As can be seen, the lower order harmonics observed in the zoomed part of **Fig. 13b** get almost canceled (voltage measurement must be ideally accurate, which is hardly viable in practice, to completely suppress these harmonics), whereas an excellent matching can be observed in the higher part of the spectrum.

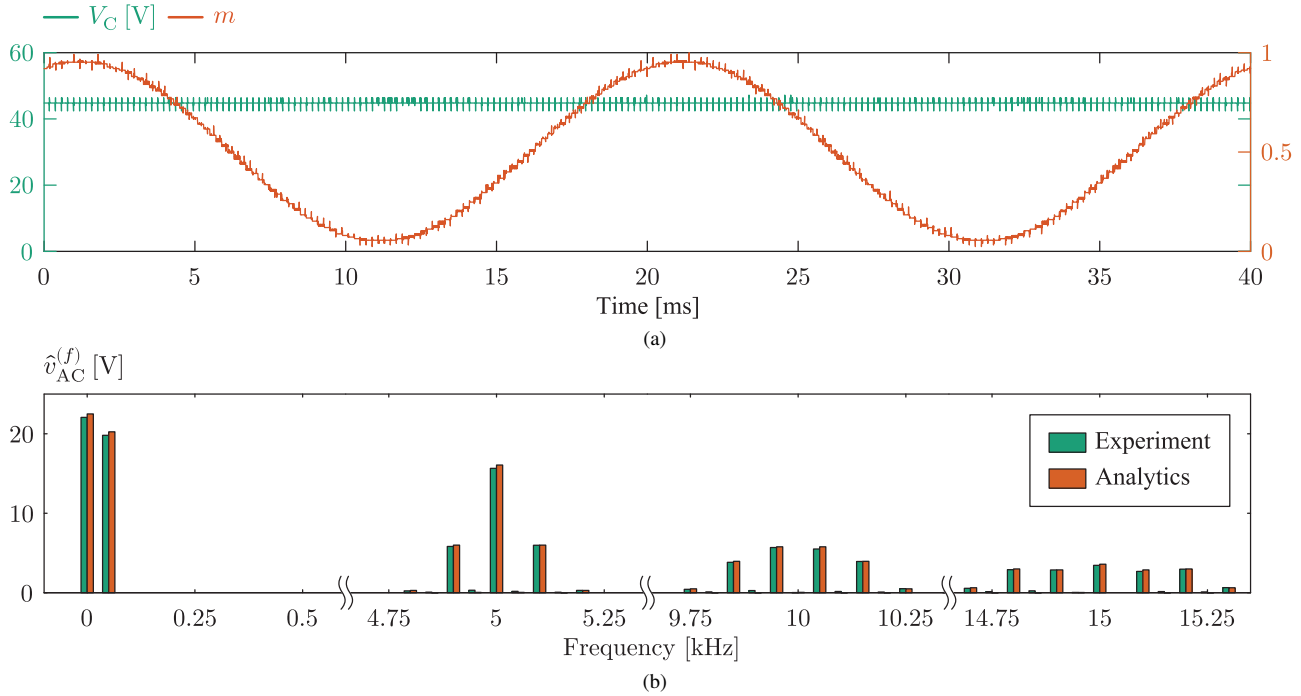

Fig. 12. (a) HB module DC link voltage V_{C} along with the modulation signal m; (b) Comparison between spectral components of the voltage measured across the module's AC terminals and the results obtained through the use of the analytic expression derived within the paper; In this case, no DC link oscillations are observed, which corresponds to the cases already covered in the literature.

This article has been accepted for publication in a future issue of this journal, but has not been fully edited. Content may change prior to final publication. Citation information: DOI 10.1109/TPEL.2020.2996418, IEEE Transactions on Power Electronics

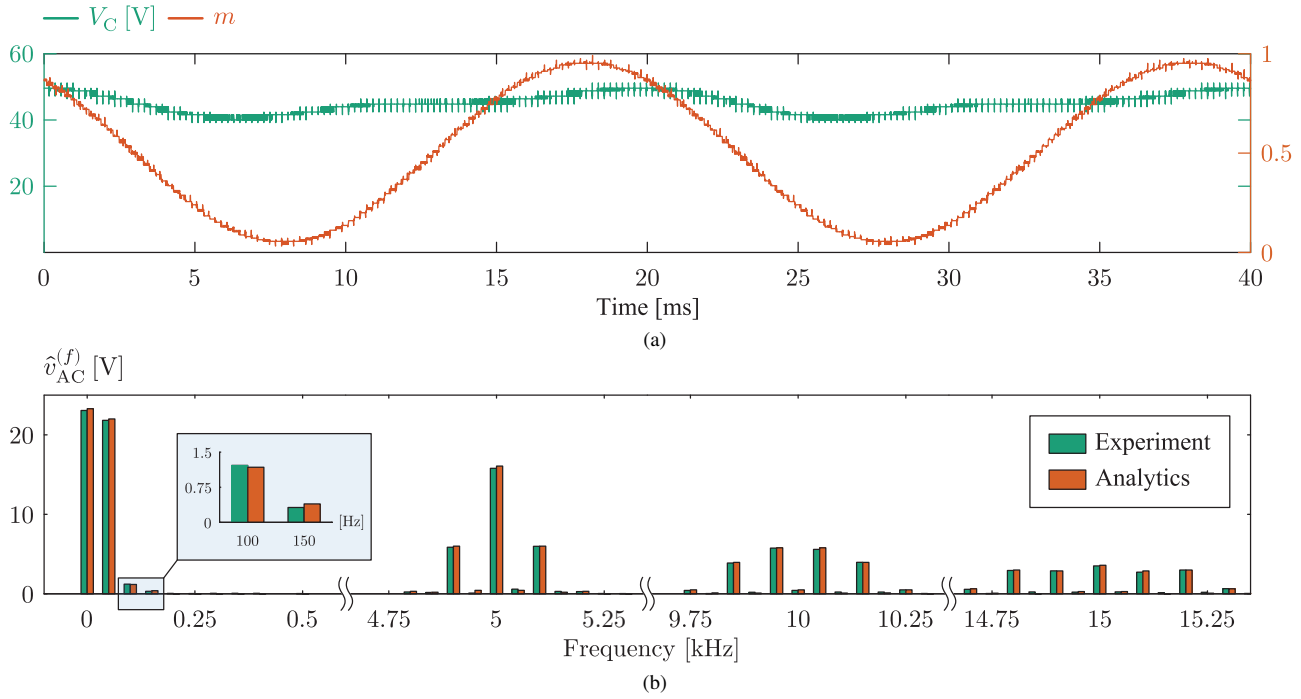

Fig. 13. (a) HB module DC link voltage V_C along with the modulation signal m; (b) Comparison between spectral components of the voltage measured across the module's AC terminals and the results obtained through the use of the analytic expression derived within the paper; Voltage oscillations are observed in the DC link of the employed HB module, however, these are not addressed through the modifications of modulation signal. As a consequence, low order harmonics (e.g. at 100Hz and 150Hz) can be observed in the module's AC voltage spectra.

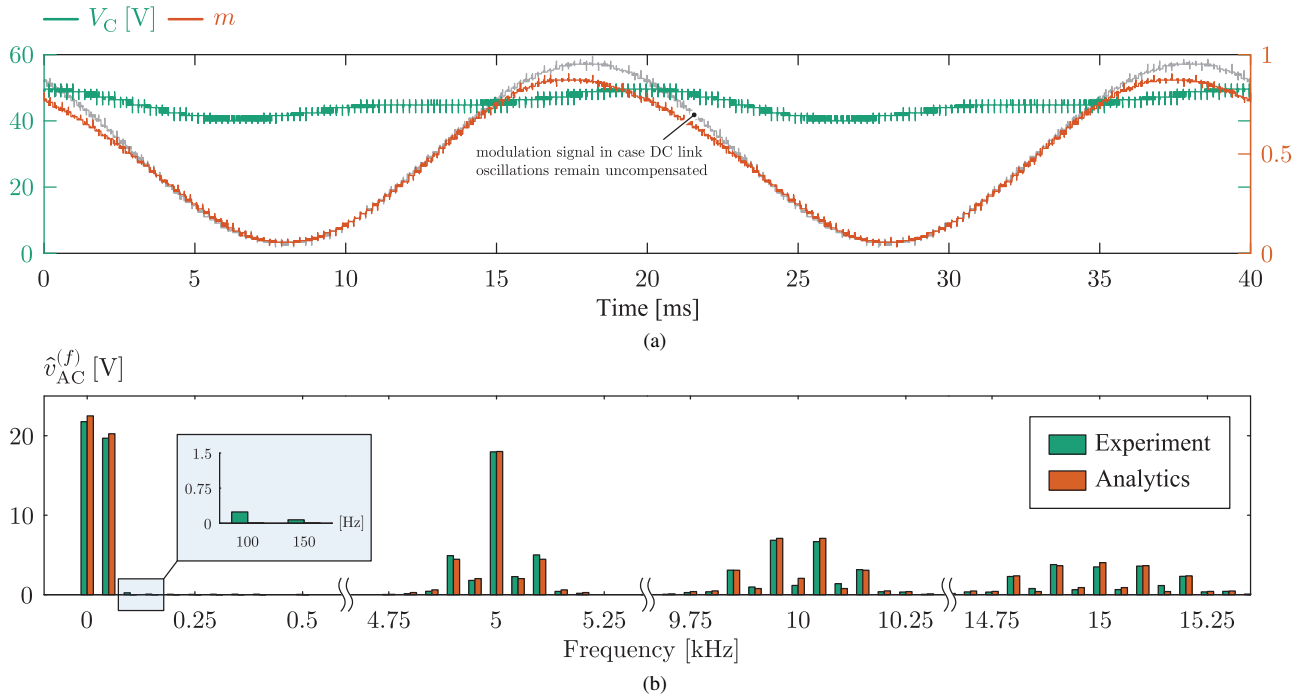

Fig. 14. (a) HB module DC link voltage V_C along with the modulation signal m; (b) Comparison between spectral components of the voltage measured across the module's AC terminals and the results obtained through the use of the analytic expression derived within the paper; In contrast to the case presented in **Fig. 13**, oscillations in the HB module DC link get compensated through the modulation signal modifications. Hence, harmonic components at 100Hz and 150Hz get almost eliminated. Please notice that complete elimination of these components requires perfect measurement of the module's DC link voltage, which was not ensured in this laboratory setup. As for higher order harmonics (up to $[15 \pm 0.25]$kHz), an excellent matching between the experimental and analytic waveforms can be observed.

V. Conclusion

In this paper, spectral analysis of PWM waveforms, generated by taking the DC link voltage oscillations into account, was presented in a comprehensive manner for the first time. A method of addressing the modulation signal modifications, required to suppress the effects of the above mentioned low frequency oscillations, was presented. Consequently, the expressions already known in the literature can be extended and modified to support the analysis of switching stages processing 1PH power at their terminals. So far, similar analyses were conducted assuming the flat DC link voltage, which is a simplification that comes at the price of hindering the calculation precision. This paper, however, provides an improvement widening the applicability of the analysis methodology used up until the present moment. Further, all the results were presented in a general form. Therefore, spectral analysis of cascaded structures relying on floating modules (such as the MMC, $\curlywedge$ or Δ STATCOM, CHB converter, etc.) can be conducted in a precise manner. Cases of both natural and regular sampling were covered in case a single HB module is observed. Nevertheless, similar reasoning can be easily applied to any type of converter building block. Correctness and outstanding precision of the presented results were experimentally demonstrated.

References

[1] D. G. Holmes and T. A. Lipo, *Pulse width modulation for power converters: principles and practice*. John Wiley & Sons, 2003, vol. 18.

[2] W. R. Bennett, "New results in the calculation of modulation products," *The Bell System Technical Journal*, vol. 12, no. 2, pp. 228–243, Apr. 1933.

[3] S. R. Bowes and B. M. Bird, "Novel approach to the analysis and synthesis of modulation processes in power convertors," *Proceedings of the Institution of Elec. Engineers*, vol. 122, no. 5, pp. 507–513, May 1975.

[4] H. Mouton and B. Putzeys, "Understanding the pwm nonlinearity: Single-sided modulation," *IEEE Trans. on Power Electronics*, vol. 27, no. 4, pp. 2116–2128, Apr. 2012.

[5] H. d. T. Mouton, B. McGrath, D. G. Holmes, and R. H. Wilkinson, "One-dimensional spectral analysis of complex pwm waveforms using superposition," *IEEE Trans. on Power Electronics*, vol. 29, no. 12, pp. 6762–6778, Dec. 2014.

[6] A. Lesnicar and R. Marquardt, "An innovative modular multilevel converter topology suitable for a wide power range," in *2003 IEEE Bologna Power Tech Conf. Proceedings,*, vol. 3, Jun. 2003, 6 pp. Vol.3-.

[7] M. Glinka and R. Marquardt, "A new ac/ac-multilevel converter family applied to a single-phase converter," in *The Fifth Int. Conf. on Power Electronics and Drive Systems, 2003. PEDS 2003.*, vol. 1, Nov. 2003, 16–23 Vol.1.

[8] P. W. Hammond, "A new approach to enhance power quality for medium voltage ac drives," *IEEE Trans. on Industry Appl.*, vol. 33, no. 1, pp. 202–208, Jan. 1997.

[9] A. Nami, J. Liang, F. Dijkhuizen, and G. D. Demetriades, "Modular multilevel converters for hvdc appl.: Review on converter cells and functionalities," *IEEE Trans. on Power Electronics*, vol. 30, no. 1, pp. 18–36, Jan. 2015.

[10] A. Antonopoulos, L. Angquist, and H.-P. Nee, "On dynamics and voltage control of the modular multilevel converter," in *Power Electronics and Appl., 2009. EPE'09. 13th European Conf. on*, IEEE, 2009, pp. 1–10.

[11] K. Ilves, S. Norrga, L. Harnefors, and H. Nee, "On energy storage requirements in modular multilevel converters," *IEEE Trans. on Power Electronics*, vol. 29, no. 1, pp. 77–88, Jan. 2014.

[12] M. Vasiladiotis, N. Cherix, and A. Rufer, "Accurate capacitor voltage ripple estimation and current control considerations for grid-connected modular multilevel converters," *IEEE Trans. on Power Electronics*, vol. 29, no. 9, pp. 4568–4579, Sep. 2014.

[13] L. Harnefors, A. Antonopoulos, K. Ilves, and H. Nee, "Global asymptotic stability of current-controlled modular multilevel converters," *IEEE Trans. on Power Electronics*, vol. 30, no. 1, pp. 249–258, Jan. 2015.

[14] K. Sharifabadi, L. Harnefors, H.-P. Nee, S. Norrga, and R. Teodorescu, *Design, control, and application of modular multilevel converters for HVDC transmission systems*. John Wiley & Sons, 2016.

[15] A. Christe and D. Dujic, "Modular multilevel converter control methods performance benchmark for medium voltage appl.," *IEEE Trans. on Power Electronics*, pp. 1–1, 2018.

[16] X. Li, Q. Song, W. Liu, S. Xu, Z. Zhu, and X. Li, "Performance analysis and optimization of circulating current control for modular multilevel converter," *IEEE Transactions on Industrial Electronics*, vol. 63, no. 2, pp. 716–727, 2016.

[17] J. Wang, J. Liang, F. Gao, X. Dong, C. Wang, and B. Zhao, "A closed-loop time-domain analysis method for modular multilevel converter," *IEEE Transactions on Power Electronics*, vol. 32, no. 10, pp. 7494–7508, 2017.

[18] K. Ilves, L. Harnefors, S. Norrga, and H. Nee, "Analysis and operation of modular multilevel converters with phase-shifted carrier pwm," *IEEE Trans. on Power Electronics*, vol. 30, no. 1, pp. 268–283, Jan. 2015.

[19] N. Hatano and T. Ise, "Control scheme of cascaded h-bridge statcom using zero-sequence voltage and negative-sequence current," *IEEE Trans. on Power Delivery*, vol. 25, no. 2, pp. 543–550, Apr. 2010.

[20] D. Karwatzki, L. Baruschka, and A. Mertens, "Survey on the hexverter topology — a modular multilevel ac/ac converter," in *2015 9th International Conference on Power Electronics and ECCE Asia (ICPE-ECCE Asia)*, Jun. 2015, pp. 1075–1082.

[21] F. Kammerer, J. Kolb, and M. Braun, "Fully decoupled current control and energy balancing of the modular multilevel matrix converter," in *2012 15th Int. Power Electronics and Motion Control Conf. (EPE/PEMC)*, Sep. 2012, LS2a.3-1-LS2a.3–8.

[22] S. Thakur, M. Odavic, A. Allu, Z. Q. Zhu, and K. Atallah, "Theoretical harmonic spectra of pwm waveforms including dc bus voltage ripple — application to low-capacitance modular multilevel converter," *IEEE Transactions on Power Electronics*, 2020.

[23] *Peb 8032 / 6-10kw – power electronic building blocks*. [Online]. Available: https : / / imperix . ch / wp - content / uploads / document / PEB8032.pdf (visited on 10/29/2019).

[24] *B-box rcp*. [Online]. Available: https://imperix.ch/products/control/bbox (visited on 10/29/2019).

[25] Seung-Gi Jeong and Min-Ho Park, "The analysis and compensation of dead-time effects in pwm inverters," *IEEE Transactions on Industrial Electronics*, vol. 38, no. 2, pp. 108–114, Apr. 1991.